Photonic Spin Hopfions and Monopole Loops

Haiwen Wang*
Department of Applied Physics, Stanford University, Stanford, California 94305, USA

Shanhui Fan†
Department of Electrical Engineering, Stanford University, Stanford, California 94305, USA

(Received 30 June 2023; accepted 28 November 2023; published 28 December 2023)

Spin textures with various topological orders are of great theoretical and practical interest. Hopfion, a spin texture characterized by a three-dimensional topological order was recently realized in electronic spin systems. Here, we show that monochromatic light can be structured such that its photonic spin exhibits a hopfion texture in the three-dimensional real space. We also provide ways to construct spin textures of arbitrary Hopf charges. When extending the system to four dimensions by introducing a parameter dimension, a new type of topological defect in the form of a monopole loop in photonic spin is encountered. Each point on the loop is a topological spin defect in three dimensions, and the loop itself carries quantized Hopf charges. Such photonic spin texture and defect may find application in control and sensing of nanoparticles, and optical generation of topological texture in motions of particles or fluids.

DOI: 10.1103/PhysRevLett.131.263801

Topological textures refer to topologically nontrivial distributions of a physical field on a geometric space [1]. A prominent example of a topological texture is the skyrmion, which describes a topologically nontrivial distribution of a physical field that can be described by a unit 3-vector, i.e., a unit vector in three-dimensional space, on a spherical surface (S^2) [2,3]. Mathematically, the skyrmion is characterized by the homotopy class of the maps from S^2 to S^2, as denoted by $\pi_2(S^2)$ [1,2]. As another example, a hopfion describes a topologically nontrivial distribution of unit 3-vectors on a three-dimensional spherical hypersurface (S^3), and is characterized by $\pi_3(S^2)$, i.e., the homotopy class of the maps from S^3 to S^2 [4–7]. The presence of topological texture is intimately related to the existence of topological defects [1]. For example, a skyrmion texture on a spherical surface implies the existence of a topological defect inside the spherical surface where the physical field vanishes [8,9].

The study of topological textures and topological defects plays a prominent role in diverse physics areas, including high-energy [10–12], condensed matter [7,13–16], and atomic physics [17]. In particular, the topological textures and topological defects for electronic spins in condensed matter systems have been extensively studied in recent years. Both skyrmions and hopfions have been observed for electronic spins [15,18,19]. These topological spin textures are of fundamental interest since they represent a topologically nontrivial elementary excitation, and they are also of practical interest since they may provide a carrier of information that is robust to perturbations [20,21].

Inspired by the development in condensed matter physics, there have been emerging interests in exploring similar topological textures and defects in photonic systems, with potential applications in sensing and imaging [9,22–27,29–37]. Similar to electrons, photons also have spin angular momentum. Skyrmion and its associated topological spin defect have been studied in photonic spin distributions [9,23–28]. There has not been, however, any work on hopfion texture in photonic spin. Moreover, the topological defect associated with the hopfion texture has not been discussed previously in either electronic or photonic systems.

In this Letter, we show that monochromatic electromagnetic wave in real three-dimensional space can be structured such that its photonic spin distribution forms a hopfion texture [Fig. 1(b)]. The topological property of the hopfion texture is manifested in the integer-valued Hopf invariant [38], referred as the Hopf charge in the following. We demonstrate the possibility of constructing photonic spin texture with arbitrary Hopf charge. When a certain parameter is included as a fourth dimension, one may encounter a Hopf defect. Passing through the defect changes the Hopf charge of the photonic spin texture by one. We note that hopfion texture has recently been demonstrated in photonics. However, these works considered polarization [36,37] or scalar phase [39] that is different from the spin angular momentum considered here.

The monochromatic electromagnetic field in real 3D space has a spin angular momentum density vector, defined as [23,27,40–47]

$$\mathbf{S} = \frac{1}{4\omega}[\epsilon_0 \mathrm{Im}(\mathbf{E}^* \times \mathbf{E}) + \mu_0 \mathrm{Im}(\mathbf{H}^* \times \mathbf{H})], \qquad (1)$$

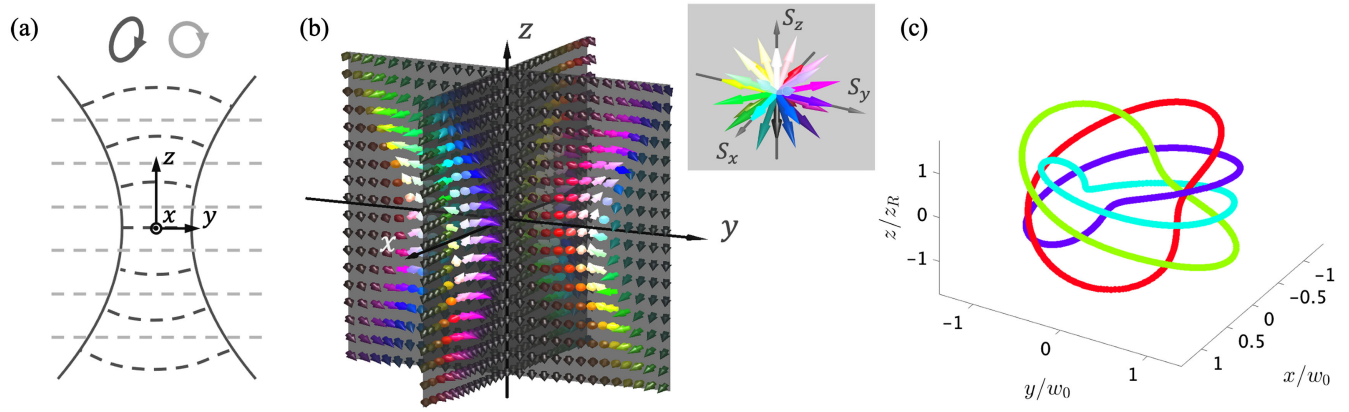

FIG. 1. Photonic spin hopfion and its creation. (a) Schematic of the structured beam described by Eq. (5). All beams propagates in the $+z$ direction. The Gaussian beam (dark lines) is a superposition of the LCP and RCP components. The plane wave (gray dashed lines) has right-circular polarization. (b) The distribution of normalized spin vector $\mathbf{n}$ in 3D real space for the beam configuration in (a). The orientation of the vector is color coded according to the inset on the top right. For better visual clarity, the vector here is obtained from the original vector by dividing S_z by 3 and rescaling such vector to unit length. (c) Lines in real space on which the spin orientation is constant. The spin orientations and its color are (1,0,0), cyan; (0,1,0), purple; $(0,-1,0)$, green; and $(-1,0,0)$, red.

where $\mathbf{E}$ and $\mathbf{H}$, respectively, are complex vectors of electric field and magnetic field, ϵ_0 and μ_0, respectively, are the vacuum permittivity and permeability, and ω is the angular frequency of the light. Using the spin density vector, one can define a normalized spin vector $\mathbf{n} = \mathbf{S}/|\mathbf{S}|$ that takes value on the unit sphere S^2.

A hopfion texture of photonic spin can be constructed as follows. We consider a monochromatic beam propagating in the $+z$ direction. The transverse (x, y) components of the electric field can be written as

$$\begin{aligned}\mathbf{E}_t &= u_1 e^{ikz}(\mathbf{e}_x - i\mathbf{e}_y) + u_2 e^{ikz}(\mathbf{e}_x + i\mathbf{e}_y)\\ &= (u_1 e^{-i\theta} + u_2 e^{i\theta})e^{ikz}\mathbf{e}_r + (-iu_1 e^{-i\theta} + iu_2 e^{i\theta})e^{ikz}\mathbf{e}_\theta,\end{aligned} \tag{2}$$

where u_1 and u_2 are the slowly varying envelope function of right-circular polarization (RCP) and left-circular polarization (LCP) components, respectively. $k = 2\pi/\lambda$ is the wave vector. λ is the wavelength. $\mathbf{e}_{x,y,r,\theta}$ are unit vectors along the respective coordinate axis. r and θ are cylindrical coordinates defined as $r = \sqrt{x^2 + y^2}$, $\theta = \arctan(y/x)$. The transverse components of the magnetic field are

$$\mathbf{H}_t = \frac{1}{Z_0}[(iu_1 e^{-i\theta} - iu_2 e^{i\theta})e^{ikz}\mathbf{e}_r + (u_1 e^{-i\theta} + u_2 e^{i\theta})e^{ikz}\mathbf{e}_\theta]. \tag{3}$$

Z_0 is the vacuum impedance. The field in the longitudinal (z) direction is obtained by satisfying Gauss's law $\nabla \cdot \mathbf{E} = 0$ and $\nabla \cdot \mathbf{H} = 0$ to first order [48,49]:

$$\begin{aligned}E_z &= \frac{i}{kr}\left[\frac{\partial(rE_r)}{\partial r} + \frac{\partial E_\theta}{\partial \theta}\right]\\ H_z &= \frac{i}{kr}\left[\frac{\partial(rH_r)}{\partial r} + \frac{\partial H_\theta}{\partial \theta}\right]\end{aligned} \tag{4}$$

We first analyze a simple example that lead to a hopfion texture. As we will explain below, various general considerations for creating and engineering such spin texture can be seen from this simple example. We choose

$$\begin{aligned}u_1 &= -0.7 + 4.5u_g\\ u_2 &= 1.5u_g\end{aligned} \tag{5}$$

where u_g is the Gaussian beam envelope, given by

$$u_g(r,\theta,z) = -i\sqrt{\frac{2z_R}{\lambda}}\frac{1}{z - iz_R}\exp\left[\frac{ikr^2}{2(z - iz_R)}\right]. \tag{6}$$

z_R is the Rayleigh range of the beam, taken to be 20λ throughout this Letter. The constant -0.7 in u_1 represents a plane-wave component. Such beam configuration is schematically shown in Fig. 1(a), where we superpose the LCP and RCP component with the same Gaussian profile and represent the beam as elliptically polarized.

The spin texture from such beam configuration is plotted in Fig. 1(b). As we will show below, the spin texture is rotationally symmetric around the z axis. For points on the z axis or sufficiently far away from the origin, the spin density points to the $-z$ direction. The former is because the z component of the fields is zero on axis, and the latter is because $u_g \to 0$ sufficiently far from the origin. In the semi-infinite plane of constant θ (referred to as the rz plane in the following), there is a point $r = r_0$, $z = 0$ where the spin

points to the $+z$ direction [white arrow in Fig. 1(b)]. In a 2D region on the rz plane around such point, the spin forms a skyrmion texture. Such point is referred to as the center of the skyrmion below. As θ vary from 0 to 2π, the skyrmion texture "co-rotates" with θ, producing a rotationally invariant 3D texture, known as a twisted skyrmion loop [50]. One can also trace the position of a given spin orientation in space [Fig. 1(c)]. Their trajectories form a pairwise linked loop, where the linking number equals the Hopf charge [38,51]. Such linking behavior and the twisted skyrmion loop are signatures of a hopfion texture [15,51].

The spin texture here is defined in 3D real space. Since the plane-wave component ensures the spin vector sufficiently far away from the origin approaches the same vector, the 3D real space can be compactified into a 3-sphere S^3. The hopfion texture can then be classified by the homotopy group $\pi_3(S^2) = Z$, describing topologically distinct classes of maps from S^3 to S^2 [1,4,7,14,52]. The Hopf charge, being the topological invariant of this map, is given by [36,38,53]

$$Q = \int_V \mathbf{A} \cdot \mathbf{B} \mathrm{d}^3 x \tag{7}$$

Here, $\mathbf{B}$ is known as the emergent magnetic field, or skyrmion density, defined as $B_i = (1/8\pi)\epsilon_{ijk}\mathbf{n} \cdot (\partial_j \mathbf{n} \times \partial_k \mathbf{n})$, where i, j, k denote real space indices [2,9], and $\mathbf{A}$ is the 'vector potential' of $\mathbf{B}$ satisfying $\nabla \times \mathbf{A} = \mathbf{B}$. Duplicate indices indicate summation. The integration domain V is the whole 3D space. We note that such expression of Hopf charge has a similar form with the optical helicity [54] or the magnetic helicity [52], although the physical context is completely different.

To understand the construction of such spin texture, we plot the amplitude and phase of the function u_1 in Figs. 2(a) and 2(b), respectively. We see that near $r/w_0 \approx 1$ and $z = 0$, the amplitude of u_1 goes to zero and its phase shows a vortex around such zero. In contrast, u_2, being a Gaussian envelope, does not have any zeros or phase singularities. The location of the vortex therefore approximately determines the center of the skyrmion texture in the rz plane. This relation between the phase vortex and the skyrmion texture in the rz plane underlies our construction of a hopfion texture in this example.

Building upon the understanding of the specific example of Eq. (5), we next discuss the general criterion for the choice of u_1 and u_2 in Eq. (2) that leads to a Hopfion texture. We calculate the spin distribution of a field given by Eqs. (2)–(4), using Eq. (1):

$$\begin{aligned} S_r &= \frac{\epsilon_0}{k\omega}(\mathrm{Im}f_1 + \mathrm{Im}f_2) \\ S_\theta &= \frac{\epsilon_0}{k\omega}(\mathrm{Re}f_1 - \mathrm{Re}f_2) \\ S_z &= \frac{\epsilon_0}{k\omega}(|u_2|^2 - |u_1|^2), \end{aligned} \tag{8}$$

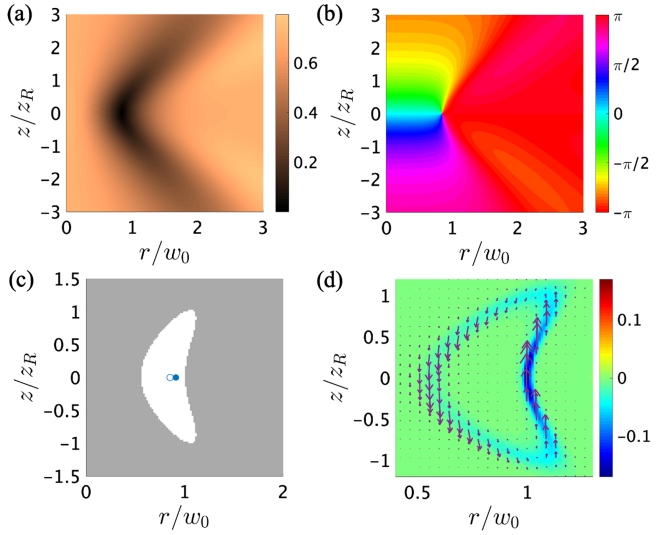

FIG. 2. General rules for constructing a photonic spin hopfion. The amplitude (a) and the phase (b) of the envelope function u_1 in Eq. (5). (c) The region where $S_z > 0$ (white) and $S_z \leq 0$ (gray). Circle represents the phase singularity point of f_1. Solid dot represents the point where $S_r = S_\theta = 0$. The spin is purely in $+z$ direction. (d) Emergent magnetic field in the rz plane. B_r and B_z components are shown in purple arrows, and B_θ component is shown in color plot. Negative B_θ components points from the paper towards the reader.

where

$$\begin{aligned} f_1 &= u_1^* \left(-\frac{\partial u_1}{\partial r} + \frac{i}{r}\frac{\partial u_1}{\partial \theta} \right) \\ f_2 &= u_2^* \left(\frac{\partial u_2}{\partial r} + \frac{i}{r}\frac{\partial u_2}{\partial \theta} \right). \end{aligned} \tag{9}$$

In our general construction criteria, we choose u_1 to be a superposition of Laguerre Gaussian modes [55,56] with azimuthal index $m_1 = 0$ and a plane-wave component. We choose u_2 to be a superposition of Laguerre Gaussian modes with the same azimuthal index m_2. If we choose $m_2 = 0$, a small plane-wave component that is smaller than the plane-wave component for u_1 may be included in the superposition. We see that Eq. (5) fits into our general choice here. Under this general choice of u_1 and u_2, the spin component S_r, S_θ, S_z does not explicitly depend on θ, since in Eq. (9), all $\exp(im\theta)$ dependency is cancelled. Therefore, such spin texture is rotationally invariant. If we choose the envelope function u_2 to be small enough, for most of the spatial locations including infinity, $|u_1| > |u_2|$ and therefore $S_z < 0$ [gray region in Fig. 2(c)]. In general, u_2 is nonzero around the zero of u_1. Therefore, around each zero of u_1 we have a finite region where $S_z > 0$ [white region in Fig. 2(c)]. Each region contains only one zero of u_1 if we choose a sufficiently small u_2. If u_2 is also sufficiently slow-varying, we have $|f_2| \ll |f_1|$. Note that if u_2 represents a plane wave, $f_2 = 0$. When f_2 is negligibly

small, S_r and S_θ are approximately the imaginary and real part of a complex function f_1, which equals to zero when $u_1 = 0$. At these points, we have the spin inversion (i.e., spin being completely in the $+z$ direction). Around such zeros of f_1, the phase vortex leads to a winding in the S_r and S_θ component. Such winding and the spin inversion point lead to a skyrmion texture in the rz plane.

Although ideally we require u_2 to be sufficiently small and slow-varying, in practice, we found that u_2 being a fraction of the amplitude of u_1 [see Eq. (5)] suffices to create a skyrmion texture in the rz plane and therefore a hopfion texture in 3D space. In Fig. 2(c), we use "o" to represent the zero of f_1, and use solid dot to represent the point where $S_r = S_\theta = 0$. The two points are close in position. In fact, one can view f_2 as a small perturbation added onto f_1 that will not destroy the phase singularity, but only shifts it slightly. As long as the perturbation is small such that the solid dot stays in the region where $S_z > 0$ (white region), the skyrmion texture in the rz plane and hence the hopfion texture in 3D remains.

We numerically calculate the Hopf charge of photonic spin texture [Fig. 1(b)] for the beam configuration given by Eq. (5). We first calculate the emergent magnetic field $\mathbf{B}$ and then solve for the $\mathbf{A}$ under the gauge choice $\nabla \cdot \mathbf{A} = 0$. Such calculation can be done conveniently in the spatial frequency domain [16]. Numerically integrating Eq. (7) indicates a Hopf charge of $+1$. This is consistent with the fact that the field lines of $\mathbf{B}$, which is also the line of constant spin orientation in Fig. 1(c), have a positive (right-handed) helicity when going along the θ direction. This indicates a positive Hopf charge [57]. Any two of the field lines also has a linking number 1. Therefore, such configuration has a Hopf charge $+1$.

Because of the correspondence between the phase vortices of u_1 and the skyrmion texture of photonic spin in the rz plane, one can in fact create photonic spin textures of arbitrary Hopf charge by engineering the phase vortices of u_1. We provide such a construction and examples in the Supplemental Material [53].

We now proceed to demonstrate the topological defect that is closely related to such topological texture, known as the Hopf defect [11,58]. Hopf defect appears in four dimensions. Pointlike Hopf defects are usually unstable against perturbations. As a result of perturbations, it deforms into a ring, known as the monopole loop [11,58]. Each point on the loop is a monopolelike defect in a three dimensional space that does not include the tangential direction of the loop. When the monopole points form loop in four dimensions, the entire loop can be regarded as a Hopf defect and carries integer Hopf charges. We illustrate the formation of monopole loops in the Supplemental Material [53]. An analogous phenomenon known as disclination ring that occurs in 3D space was found in liquid crystals [59] and systems with non-Hermitian Hamiltonians [60].

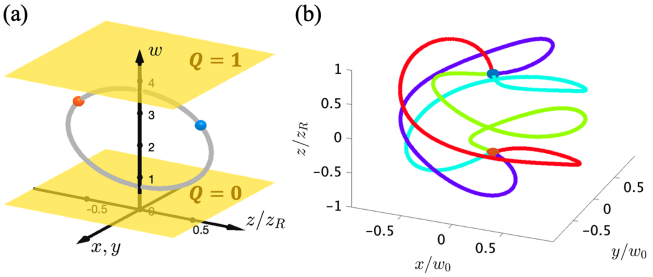

FIG. 3. Photonic spin defect in 3D and 4D spaces. (a) Schematic of the loop that consists of points of photonic spin defect (gray) in 4D space (x, y, z, w). The upper plane at $w = 4.5$ has photonic spin texture in xyz space with Hopf charge $+1$. The lower plane at $w = 0.5$ has photonic spin texture in xyz space with Hopf charge 0. Red and blue dots represent two representative points on the monopole loop ($w = 3.0$), and have skyrmion numbers $+1$ and -1, respectively. (b) The same pair of defect points in xyz space. $w = 3.0$. The spin orientation is constant along each colored line, with the color scheme the same as Fig. 1(c).

One can realize the monopole loop in photonic spin density distribution by introducing a parameter dimension to be the fourth dimension. As an example, we introduce a parameter w by modifying Eq. (5) as

$$u_1 = -0.7 + w u_g$$
$$u_2 = 1.5 u_g. \tag{10}$$

When $w = 4.5$, this is the previously studied case where the spin exhibits a charge 1 hopfion texture [upper plane in Fig. 3(a)]. When decreasing w to 3.71, a pair of monopole-like singularities start to appear on the z axis [Fig. 3(a)]. For such singularities, the spin vanishes at a specific point in 3D real space. And on a spherical surface around that point the spin has a skyrmion texture. Such singularities are known as topological spin defect, and are classified by the skyrmion number of that texture [9]. The skyrmion number is -1 for the blue dot and $+1$ for the red dot. This is further illustrated in Fig. 3(b). The lines of constant spin, which are also the emergent magnetic field lines, form a dipolelike structure. Further decreasing w to 0.71, two spin defect points annihilate each other. Therefore, the defects form a loop in 4D space. At $w = 0.5 < 0.71$, the Hopf charge of the spin texture in 3D real space is zero [lower plane in Fig. 3(a)]. Comparing this case with the case where $w = 4.5$, we see that the monopole spin defect loop carries unity Hopf charge and is therefore topologically equivalent to a Hopf defect. For spin texture with higher Hopf charge, passing through a monopole loop also changes the Hopf charge by unity [53]. To the authors' knowledge, such monopole loop was not previously discussed in the spin texture of any system.

Our work shows that photons can exhibit a hopfion spin texture. These results certainly have connections to hopfion spin texture for electrons. But photons and electrons are

different fundamental particles, and their spin properties have different physical manifestations. The Stokes vector, a real vector calculated from the local polarization state of light (often known as pseudospin) was also shown recently to form hopfion textures [36,37]. However, we point out that the spin density and the Stokes vector are different quantities and there is no straightforward relation between the polarization Hopf charge and the spin Hopf charge. In fact, the spin hopfion texture presented above has a zero Hopf charge in its Stokes vector. We provide more discussion in the Supplemental Material [53].

We envision that such spin texture can be experimentally measured by analyzing the scattering from a probe particle [49]. Considering the mechanical effect, the spin density gives rise to a torque to such particles inside the electromagnetic field [9,42,61]. Given that the cross section of a spin hopfion contains skyrmions, the torque on the particle may be oriented along arbitrary direction by changing the relative position between the beam and the particle. It is also conceivable to collectively rotate many particles to imprint the hopfion texture onto their rotation axes, therefore potentially creating topological textures in the vorticity of a fluid flow [62].

Spin density occurs in many other types of waves, including electron waves [63], acoustic waves [64], and surface gravity waves [65]. Besides spin, there may be other quantities of field, such as the linear momentum or the orbital angular momentum, that contribute to wave-matter interaction [43,66]. This work points to the potential in engineering topological textures in spin density and possibly other quantities of various waves.

In summary, we point out that the spin density of monochromatic light can form hopfion textures. The hopfion texture, which can be viewed as a twisted skyrmion loop, can be created by engineering the vortices in one of the envelope functions of the beam. We provide examples to construct photonic spin hopfion texture of unity and higher Hopf charges. By introducing a parameter dimension, we encounter monopole loops as the topological defect that separates photonic spin texture of different Hopf charges. Such topological defects and textures may allow new ways of controlling nanoparticles, may be used to generate topological texture in the motion of particles or the flow of fluids, and point to the possibility of engineering topological textures in other types of waves.

This work is supported by a MURI grant from the U.S. Office of Naval Research (Grant No. N00014-20-1-2450).

*hwwang@stanford.edu
†shanhui@stanford.edu

[1] N. D. Mermin, The topological theory of defects in ordered media, Rev. Mod. Phys. **51**, 591 (1979).
[2] J. H. Han, *Skyrmions in Condensed Matter* (Springer, New York, 2017), Vol. 278.
[3] B. A. Bernevig, Topological insulators and topological superconductors, in *Topological Insulators and Topological Superconductors* (Princeton University Press, Princeton, NJ, 2013).
[4] H. Hopf, Über die abbildungen der dreidimensionalen sphäre auf die kugelfläche, Math. Ann. **104**, 637 (1931).
[5] A. Hatcher, *Algebraic Topology* (Cambridge University Press, Cambridge, England, 2002).
[6] H. Urbantke, The Hopf fibration–seven times in physics, J. Geom. Phys. **46**, 125 (2003).
[7] J.-S. Wu and I. I. Smalyukh, Hopfions, heliknotons, skyrmions, torons and both Abelian and non-Abelian vortices in chiral liquid crystals, Liq. Cryst. Rev. **10**, 34 (2022).
[8] P. Milde, D. Köhler, J. Seidel, L. Eng, A. Bauer, A. Chacon, J. Kindervater, S. Mühlbauer, C. Pfleiderer, S. Buhrandt *et al.*, Unwinding of a skyrmion lattice by magnetic monopoles, Science **340**, 1076 (2013).
[9] H. Wang, C. C. Wojcik, and S. Fan, Topological spin defects of light, Optica **9**, 1417 (2022).
[10] L. Faddeev and A. J. Niemi, Stable knot-like structures in classical field theory, Nature (London) **387**, 58 (1997).
[11] F. Bruckmann, Hopf defects as seeds for monopole loops, J. High Energy Phys. 08 (2001) 030.
[12] N. Manton and P. Sutcliffe, *Topological solitons* (Cambridge University Press, Cambridge, England, 2004).
[13] Bryan Gin-ge Chen, P. J. Ackerman, G. P. Alexander, R. D. Kamien, and I. I. Smalyukh, Generating the Hopf fibration experimentally in nematic liquid crystals, Phys. Rev. Lett. **110**, 237801 (2013).
[14] P. J. Ackerman and I. I. Smalyukh, Static three-dimensional topological solitons in fluid chiral ferromagnets and colloids, Nat. Mater. **16**, 426 (2017).
[15] N. Kent, N. Reynolds, D. Raftrey, I. T. Campbell, S. Virasawmy, S. Dhuey, R. V. Chopdekar, A. Hierro-Rodriguez, A. Sorrentino, E. Pereiro *et al.*, Creation and observation of Hopfions in magnetic multilayer systems, Nat. Commun. **12**, 1562 (2021).
[16] J. E. Moore, Y. Ran, and X.-G. Wen, Topological surface states in three-dimensional magnetic insulators, Phys. Rev. Lett. **101**, 186805 (2008).
[17] W. Lee, A. H. Gheorghe, K. Tiurev, T. Ollikainen, M. Möttönen, and D. S. Hall, Synthetic electromagnetic knot in a three-dimensional skyrmion, Sci. Adv. **4**, eaao3820 (2018).
[18] S. Muhlbauer, B. Binz, F. Jonietz, C. Pfleiderer, A. Rosch, A. Neubauer, R. Georgii, and P. Boni, Skyrmion lattice in a chiral magnet, Science **323**, 915 (2009).
[19] X. Yu, Y. Onose, N. Kanazawa, J. H. Park, J. Han, Y. Matsui, N. Nagaosa, and Y. Tokura, Real-space observation of a two-dimensional skyrmion crystal, Nature (London) **465**, 901 (2010).
[20] J. Iwasaki, M. Mochizuki, and N. Nagaosa, Current-induced skyrmion dynamics in constricted geometries, Nat. Nanotechnol. **8**, 742 (2013).
[21] A. Fert, N. Reyren, and V. Cros, Magnetic skyrmions: Advances in physics and potential applications, Nat. Rev. Mater. **2**, 17031 (2017).
[22] S. Tsesses, E. Ostrovsky, K. Cohen, B. Gjonaj, N. Lindner, and G. Bartal, Optical skyrmion lattice in evanescent electromagnetic fields, Science **361**, 993 (2018).

[23] L. Du, A. Yang, A. V. Zayats, and X. Yuan, Deep-subwavelength features of photonic skyrmions in a confined electromagnetic field with orbital angular momentum, Nat. Phys. **15**, 650 (2019).
[24] X. Lei, A. Yang, P. Shi, Z. Xie, L. Du, A. V. Zayats, and X. Yuan, Photonic spin lattices: symmetry constraints for skyrmion and meron topologies, Phys. Rev. Lett. **127**, 237403 (2021).
[25] X. Lei, L. Du, X. Yuan, and A. V. Zayats, Optical spin–orbit coupling in the presence of magnetization: Photonic skyrmion interaction with magnetic domains, Nanophotonics **10**, 3667 (2021).
[26] M. Lin, W. Zhang, C. Liu, L. Du, and X. Yuan, Photonic spin skyrmion with dynamic position control, ACS Photonics **8**, 2567 (2021).
[27] Y. Dai, Z. Zhou, A. Ghosh, R. S. Mong, A. Kubo, C.-B. Huang, and H. Petek, Plasmonic topological quasiparticle on the nanometre and femtosecond scales, Nature (London) **588**, 616 (2020).
[28] Y. Shen, Q. Zhang, P. Shi, L. Du, A. V. Zayats, and X. Yuan, Topological quasiparticles of light: optical skyrmions and beyond, arXiv:2205.10329.
[29] T. J. Davis, D. Janoschka, P. Dreher, B. Frank, F.-J. Meyer zu Heringdorf, and H. Giessen, Ultrafast vector imaging of plasmonic skyrmion dynamics with deep subwavelength resolution, Science **368**, eaba6415 (2020).
[30] S. Gao, F. C. Speirits, F. Castellucci, S. Franke-Arnold, S. M. Barnett, and J. B. Götte, Paraxial skyrmionic beams, Phys. Rev. A **102**, 053513 (2020).
[31] C. Guo, M. Xiao, Y. Guo, L. Yuan, and S. Fan, Meron spin textures in momentum space, Phys. Rev. Lett. **124**, 106103 (2020).
[32] C. Guo, M. Xiao, M. Orenstein, and S. Fan, Structured 3d linear space–time light bullets by nonlocal nanophotonics, Light **10**, 160 (2021).
[33] Y. Shen, Y. Hou, N. Papasimakis, and N. I. Zheludev, Supertoroidal light pulses as electromagnetic skyrmions propagating in free space, Nat. Commun. **12**, 5891 (2021).
[34] Y. Shen, Topological bimeronic beams, Opt. Lett. **46**, 3737 (2021).
[35] Y. Shen, E. C. Martínez, and C. Rosales-Guzmán, Generation of optical skyrmions with tunable topological textures, ACS Photonics **9**, 296 (2022).
[36] D. Sugic, R. Droop, E. Otte, D. Ehrmanntraut, F. Nori, J. Ruostekoski, C. Denz, and M. R. Dennis, Particle-like topologies in light, Nat. Commun. **12**, 6785 (2021).
[37] Y. Shen, B. Yu, H. Wu, C. Li, Z. Zhu, and A. V. Zayats, Topological transformation and free-space transport of photonic hopfions, Adv. Photonics. **5**, 015001 (2023).
[38] J. Whitehead, An expression of Hopf's invariant as an integral, Proc. Natl. Acad. Sci. U.S.A. **33**, 117 (1947).
[39] C. Wan, Y. Shen, A. Chong, and Q. Zhan, Scalar optical Hopfions, eLight **2**, 22 (2022).
[40] S. M. Barnett, Rotation of electromagnetic fields and the nature of optical angular momentum, J. Mod. Opt. **57**, 1339 (2010).
[41] K. Y. Bliokh, A. Y. Bekshaev, and F. Nori, Extraordinary momentum and spin in evanescent waves, Nat. Commun. **5**, 3300 (2014).
[42] A. Y. Bekshaev, K. Y. Bliokh, and F. Nori, Transverse spin and momentum in two-wave interference, Phys. Rev. X **5**, 011039 (2015).
[43] K. Y. Bliokh and F. Nori, Transverse and longitudinal angular momenta of light, Phys. Rep. **592**, 1 (2015).
[44] K. Y. Bliokh, F. J. Rodríguez-Fortuño, F. Nori, and A. V. Zayats, Spin–orbit interactions of light, Nat. Photonics **9**, 796 (2015).
[45] K. Y. Bliokh, A. Y. Bekshaev, and F. Nori, Optical momentum, spin, and angular momentum in dispersive media, Phys. Rev. Lett. **119**, 073901 (2017).
[46] K. Y. Bliokh, A. Y. Bekshaev, and F. Nori, Optical momentum and angular momentum in complex media: From the Abraham–Minkowski debate to unusual properties of surface plasmon-polaritons, New J. Phys. **19**, 123014 (2017).
[47] D. Sugic, M. R. Dennis, F. Nori, and K. Y. Bliokh, Knotted polarizations and spin in three-dimensional polychromatic waves, Phys. Rev. Res. **2**, 042045(R) (2020).
[48] A. Y. Bekshaev and M. Soskin, Transverse energy flows in vectorial fields of paraxial beams with singularities, Opt. Commun. **271**, 332 (2007).
[49] M. Neugebauer, J. S. Eismann, T. Bauer, and P. Banzer, Magnetic and electric transverse spin density of spatially confined light, Phys. Rev. X **8**, 021042 (2018).
[50] P. Sutcliffe, Let's twist again, Nat. Mater. **16**, 392 (2017).
[51] F. Wilczek and A. Zee, Linking numbers, spin, and statistics of solitons, Phys. Rev. Lett. **51**, 2250 (1983).
[52] C. B. Smiet, S. Candelaresi, A. Thompson, J. Swearngin, J. W. Dalhuisen, and D. Bouwmeester, Self-organizing knotted magnetic structures in plasma, Phys. Rev. Lett. **115**, 095001 (2015).
[53] See Supplemental Material at http://link.aps.org/supplemental/10.1103/PhysRevLett.131.263801 for a heuristic derivation of the Hopf charge, methods and examples for constructing photonic spin texture of arbitrary Hopf charges, relation between Hopf defects and monopole loops, transition between higher order hopfion textures, and discussion about photonic spin hopfion and Stokes vector hopfion.
[54] R. P. Cameron, S. M. Barnett, and A. M. Yao, Optical helicity, optical spin and related quantities in electromagnetic theory, New J. Phys. **14**, 053050 (2012).
[55] A. E. Siegman, *Lasers* (University Science Books, Sausalito, California, 1986).
[56] G. Vallone, On the properties of circular beams: Normalization, Laguerre-Gauss expansion, and free-space divergence, Opt. Lett. **40**, 1717 (2015).
[57] A. F. Ranada and J. Trueba, Electromagnetic knots, Phys. Lett. A **202**, 337 (1995).
[58] C. Liu, F. Vafa, and C. Xu, Symmetry-protected topological Hopf insulator and its generalizations, Phys. Rev. B **95**, 161116(R) (2017).
[59] E. M. Terentjev, Disclination loops, standing alone and around solid particles, in nematic liquid crystals, Phys. Rev. E **51**, 1330 (1995).
[60] A. Cerjan, M. Xiao, L. Yuan, and S. Fan, Effects of non-hermitian perturbations on Weyl hamiltonians with arbitrary topological charges, Phys. Rev. B **97**, 075128 (2018).

[61] N. Simpson, K. Dholakia, L. Allen, and M. Padgett, Mechanical equivalence of spin and orbital angular momentum of light: An optical spanner, Opt. Lett. **22**, 52 (1997).

[62] D. Kleckner and W. T. Irvine, Creation and dynamics of knotted vortices, Nat. Phys. **9**, 253 (2013).

[63] K. Y. Bliokh, I. P. Ivanov, G. Guzzinati, L. Clark, R. Van Boxem, A. Béché, R. Juchtmans, M. A. Alonso, P. Schattschneider, F. Nori *et al.*, Theory and applications of free-electron vortex states, Phys. Rep. **690**, 1 (2017).

[64] L. Burns, K. Y. Bliokh, F. Nori, and J. Dressel, Acoustic versus electromagnetic field theory: Scalar, vector, spinor representations and the emergence of acoustic spin, New J. Phys. **22**, 053050 (2020).

[65] K. Y. Bliokh, H. Punzmann, H. Xia, F. Nori, and M. Shats, Field theory spin and momentum in water waves, Sci. Adv. **8**, eabm1295 (2022).

[66] K. Y. Bliokh, Y. P. Bliokh, and F. Nori, Ponderomotive forces, stokes drift, and momentum in acoustic and electromagnetic waves, Phys. Rev. A **106**, L021503 (2022).